A Journal of the Gesellschaft Deutscher Chemiker

Angewandte International Edition Chemie

GDCh

www.angewandte.org

Accepted Article

Title: Therapeutic Vesicular Nanoreactors with Tumor-Specific Activation and Self-Destruction for Synergistic Tumor Ablation

Authors: Junjie Li, Anjaneyulu Dirisala, Zhishen Ge, Yuheng Wang, Wei Yin, Wendong Ke, Kazuko Toh, Jinbing Xie, Yu Matsumoto, Yasutaka Anraku, Kensuke Osada, and Kazunori Kataoka

To be cited as: *Angew. Chem. Int. Ed.* 10.1002/anie.201706964
Angew. Chem. 10.1002/ange.201706964

Link to VoR: http://dx.doi.org/10.1002/anie.201706964
http://dx.doi.org/10.1002/ange.201706964

WILEY-VCH

10.1002/anie.201706964

WILEY-VCH

Therapeutic Vesicular Nanoreactors with Tumor-Specific Activation and Self-Destruction for Synergistic Tumor Ablation

Junjie Li,† Anjaneyulu Dirisala,† Zhishen Ge,* Yuheng Wang, Wei Yin, Wendong Ke, Kazuko Toh, Jinbing Xie, Yu Matsumoto, Yasutaka Anraku,* Kensuke Osada,* and Kazunori Kataoka*

Abstract: Polymeric nanoreactors (NRs) have distinct advantages to improve chemical reaction efficiency, but the *in vivo* applications were limited by lack of tissue-specificity. Herein, novel glucose oxidase (GOD)-loaded therapeutic vesicular NRs (*thera*NR) are constructed based on the diblock copolymer containing poly(ethylene glycol) (PEG) and copolymerized phenylboronic ester or piperidine-functionalized methacrylate (P(PBEM-*co*-PEM)). Upon systemic injection, *thera*NR keep inactive in normal tissues. At tumor site, *thera*NR are specifically activated by tumor acidity *via* improved permeability of the membranes. Hydrogen peroxide (H_2O_2) production by the catalysis of GOD in *thera*NR increases tumor oxidative stress significantly. Meanwhile, high level of H_2O_2 induces self-destruction of *thera*NR releasing quinone methide (QM) to deplete glutathione and suppress antioxidant ability of cancer cells. Finally, *thera*NR efficiently kill cancer cells and ablate tumor *via* the synergistic effect.

Nanoreactors (NRs) with a confined reaction space have attracted great interests to improve chemical reaction efficiency because of their wide applications in a variety of fields such as enzyme catalysis, polymerization, nanoparticle or organic synthesis, and artificial organelles.[1] Among them, therapeutic NRs have been proposed in recent years and explored to treat diseases through conversion of toxic substances into nontoxic ones to eliminate or reduce the lesions to the body, or *in situ* transformation of nontoxic prodrugs into therapeutic compounds for cell or bacteria killing.[2] Notably, NRs frequently show the distinct advantages to protect the encapsulated catalysts from the environmental media, and thereby preserving and controlling the activity.[3] Enzyme-loaded cross-linked polymeric vesicular NRs have been demonstrated to accumulate in tumor site and function as a therapeutic NR for even four days post administration to convert a model prodrug into a highly fluorescent product at the tumor site.[3b] However, the reaction may unavoidably occur in normal tissues as long as there exist NRs in main organs. Therefore, for cancer therapy, it is highly desirable to engineer therapeutic NRs that can be specifically activated at tumor site to maximize the therapeutic efficacy and minimize the adverse side effects.

Polymeric vesicles obtained from the self-assembly of amphiphilic block copolymers represent the most frequently used NRs, which possess the properties simultaneously loading hydrophilic and hydrophobic molecules within the aqueous inner cavity and hydrophobic membranes, respectively.[4] Notably, as a nanocarrier, drug release from the stimuli-responsive polymeric vesicles can be triggered by the external or internal stimuli.[5] As NRs, the reaction inside the vesicular space can also be adjusted by stimuli primarily through controlling permeability of the vesicular membranes and transportation of substrates and products.[6] However, rare stimuli-responsive polymeric vesicles were reported as smart therapeutic NRs particularly for *in vivo* applications.

Herein, as a proof of concept to construct high-efficiency therapeutic NRs for *in vivo* applications, we engineered multifunctional vesicular NRs with tumor-specific activation and self-destruction for synergistic cancer cell killing (Scheme 1). The diblock copolymers

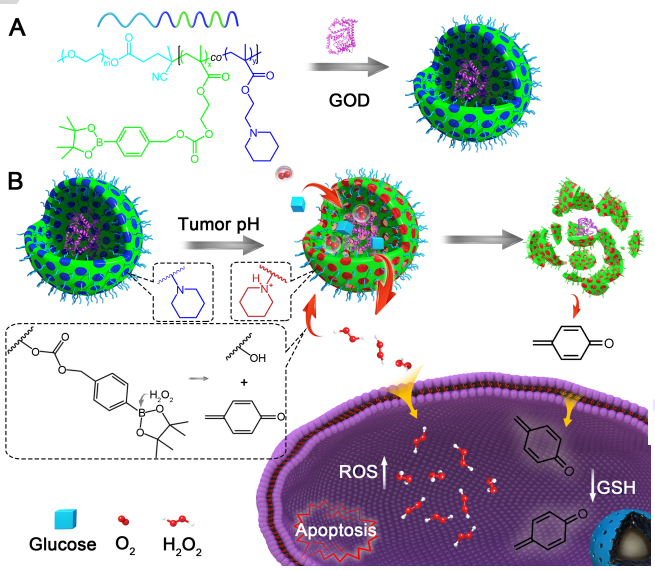

Scheme 1. Schematic illustration of (A) self-assembly of PEG-*b*-P(PBEM-*co*-PEM) to form GOD-loaded NRs (*thera*NR) and (B) the functioning mechanism of *thera*NR at tumor site including tumor pH-activation, H_2O_2 production, and QM release for synergistically killing cancer cells.

[*] J. Li, Y. Wang, W. Yin, W. Ke, Prof. Dr. Z. Ge
CAS Key Laboratory of Soft Matter Chemistry
Department of Polymer Science and Engineering
University of Science and Technology of China
Hefei, Anhui 230026, China
E-mail: gezs@ustc.edu.cn
Dr. A. Dirisala, Dr. K. Toh, Dr. J. Xie, Prof. Dr. K. Kataoka
Innovation Center of Nanomedicine, Kawasaki Institute of Industrial Promotion, 3-25-14 Tonomachi, Kawasaki-ku, Kawasaki 210-0821, Japan
Dr. Y. Anraku, Prof. Dr. K. Osada
Graduate School of Engineering, The University of Tokyo
7-3-1 Hongo, Bunkyo-ku, Tokyo 113-8656, Japan
E-mail: anraku@bmw.t.u-tokyo.ac.jp, osada@bmw.t.u-tokyo.ac.jp,
Dr. Y. Matsumoto
Department of Otorhinolaryngology and Head and Neck Surgery, Graduate School of Medicine and Faculty of Medicine, The University of Tokyo 7-3-1 Hongo, Bunkyo-ku, Tokyo 113-8655, Japan
Prof. Dr. K. Kataoka
Policy Alternatives Research Institute, The University of Tokyo 7-3-1 Hongo, Bunkyo-ku, Tokyo 113-1709, Japan
E-mail: kataoka@pari.u-tokyo.ac.jp
[†] These authors contributed equally to this work.
Supporting information for this article is given via a link at the end of the document.

composed of poly(ethylene glycol) (PEG) and copolymerized phenylboronic ester or piperidine-functionalized methacrylate (P(PBEM-*co*-PEM)) were designed and optimized *via* changing the molar ratios of PPBEM and PPEM, which could self-assemble into vesicular structure in aqueous solution at pH 7.4. After encapsulating a model enzyme, glucose oxidase (GOD), therapeutic NRs (designated as *thera*NR) were constructed. In *thera*NR, PPEM and PPBEM segments serve as tumor pH (pH 6.5-6.8) and hydrogen peroxide (H_2O_2)-responsive hydrophobic segments, respectively. At normal tissues of pH 7.4, *thera*NR maintain inactive state. After accumulation in tumor tissues, PPEM segments turn out to be hydrophilic due to protonation at tumor acidity, which endows the permeability of *thera*NR membranes and allows transportation of the nutrient small-molecule substances (glucose and oxygen). The accessibility of GOD catalyzes the oxidation reaction to produce massive H_2O_2. Accompanied by the concentration reduction of the nutrient substances, the oxidative stress in tumor tissue increases. The high concentration of H_2O_2 conversely attacks PPBEM segments and induces self-destruction of the vesicles to release quinone methide (QM) as by-products.[7] QM possesses the capability to deplete intracellular glutathione (GSH), and thus weakens the antioxidative capability of the cancer cells.[7b,8] Increasing the oxidative stress and suppressing GSH can synergistically kill cancer cells and inhibit tumor growth efficiently.

Initially, we designed the amphiphilic block copolymer, PEG-*b*-P(PBEM-*co*-PEM), for self-assembly into vesicles with pH-controllable permeability of the membranes while maintaining integrity of the vesicles. PEG-based macroRAFT agent was used to copolymerize PBEM and PEM monomers *via* reversible addition-fragmentation chain transfer (RAFT) polymerization. A series of PBEM/PEM ratios was designed and the final compositions were determined by ^{1}H NMR analysis (Figure S1, see Supporting Information (SI)). The characterization of the final polymers were summarized in Table S1 (SI). All the block copolymers were relatively narrowly distributed with M_w/M_n in the range of 1.10-1.20. Next, the block copolymers were explored to self-assemble in phosphate buffer saline (PBS, pH 7.4) upon slow addition of PBS into tetrahydrofuran (THF) solution of PEG-*b*-P(PBEM-*co*-PEM). All the block copolymers can self-assemble into well-defined vesicle morphologies with the size in the range of 100-200 nm as displayed by the transmission electron microscope (TEM) and dynamic light scattering (DLS) analysis (Figure S2, SI). TEM images show that spherical particles with high contrast between the periphery and the center indicating typical vesicular morphology. Typically, for PEG_{113}-*b*-P($PBEM_{67}$-*co*-PEM_{23}) vesicles, the particles sizes were determined to be 119 ± 31 nm from TEM images and the membrane thickness 21 ± 2.5 nm. DLS results gave the particles size of 131 nm and low polydispersity index (PDI) of 0.116. Notably, although TEM images exhibited aggregated morphology, DLS results showed well-dispersed nanoparticles in aqueous solution indicating that the aggregation in TEM images likely occurred during TEM sample preparation.[6c,6d,9]

Moreover, the interior cavity of the vesicles can be used to encapsulate hydrophilic GOD. After encapsulating GOD, they were washed with PBS to remove the unloaded free GOD. The size and size distribution of the vesicles after loading GOD nearly maintained constant (Figure 1A and Figure S3, SI). Fluorescein isothiocyanate (FITC)-labeled GOD was used and the GOD loading content was determined to be 4.7% *via* fluorescence intensity of FITC.

PEG-*b*-PPEM block copolymer has been demonstrated to exhibit pH-responsive behavior with ultrasensitivity.[10] The pK_a value of PPEM segment in PEG_{113}-*b*-P($PBEM_{67}$-*co*-PEM_{23}) was determined to be 6.95 *via* acid-base titration in aqueous solutions (Figure 1C). Thus, when the pH values were decreased from pH 7.4 to pH 6.8, PPEM segments turn out to be positively charged and hydrophilic. Next, pH-responsive behaviors of the various vesicles were studied (Figure S2, SI). The zeta-potentials of the vesicles increased with pH changing from 7.4 to 6.8 due to the protonation of PPEM segments. With PPEM contents increasing in the block copolymers, higher positive charges were observed. PEG_{113}-*b*-$PPBEM_{80}$ and PEG_{113}-*b*-P($PBEM_{67}$-*co*-PEM_{23}) vesicles showed high stability without morphological change with pH decreasing to 6.8 most likely due to low PPEM content in the block copolymers. Notably, PEG_{113}-*b*-P($PBEM_{67}$-*co*-PEM_{23}) vesicles displayed size of 122 ± 33 nm and membrane thickness of 22 ± 2.8 nm as indicated from TEM images at pH 6.8, which were similar to those at pH 7.4. In sharp contrast, PEG_{113}-*b*-$PPEM_{70}$ and PEG_{113}-*b*-

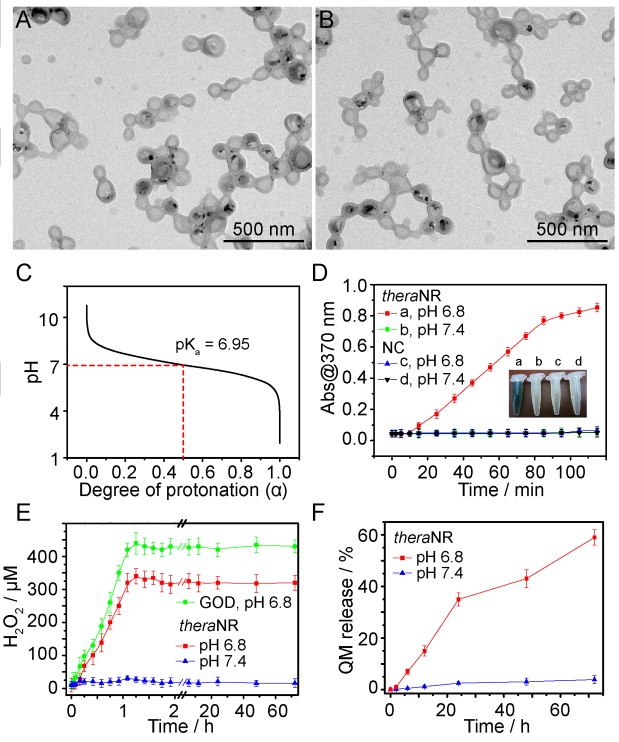

Figure 1. (A) TEM images of *thera*NR at pH 7.4 and (B) *thera*NR at pH 6.8. (C) Acid-base titration curve of PEG_{113}-*b*-P($PBEM_{67}$-*co*-PEM_{23}). (D) Absorbance (abs, 370 nm) of the product (oxidative TMB) after cascade reactions in *thera*NR or NC solution loading GOD (100 mU/mL) in the presence of glucose (1 mg/mL), HRP (150 mU/mL), and TMB (100 μM) outside the vesicles at pH 7.4 or pH 6.8. (E) H_2O_2 production of *thera*NR or GOD (100 mU/mL GOD) in the presence of 1 mg/mL glucose at pH 7.4 or pH 6.8. (F) QM release from *thera*NR (100 mU/mL GOD) in the presence of 1 mg/mL glucose at pH 7.4 or pH 6.8. Mean ± s.d., n = 3.

P(PBEM$_{65}$-*co*-PEM$_{40}$) vesicles lost the integrity at pH 6.8 as observed in the TEM images. According to our aim for tumor acidity activation of the nanoreactors and protection of the encapsulated enzymes by the vesicles for a period of time, GOD-loaded PEG$_{113}$-*b*-P(PBEM$_{67}$-*co*-PEM$_{23}$) vesicles were selected for further investigation due to the suitable PPEM content, which were denoted as *thera*NR. Note that, *thera*NR showed similar morphologies and particle sizes at pH 6.8 and pH 7.4 (Figure 1A,B). The GOD-loaded PEG$_{113}$-*b*-PPBEM$_{80}$ vesicles were used as a control of the nanocarrier without pH-responsiveness (NC).

Next, we further evaluated the pH-responsive permeability variation of *thera*NR through the cascade reaction of glucose oxidation by GOD to generate H_2O_2 and subsequent reaction with 3,3',5,5'-tetramethylbenzidine (TMB) and horseradish peroxidase (HRP).[11] Glucose, TMB, and HRP were localized in the exterior environment of the vesicles, thus the permeability of the vesicles can be determined by monitoring the characteristic absorbance of oxidized TMB.[12] TMB, glucose, and HRP were added into *thera*NR solution at pH 7.4, followed by adjusting pH to 6.8. Apparently, the color of *thera*NR solution became blue and the absorbance at 370 nm increased rapidly indicating high permeability of the vesicle membranes (Figure 1D). However, the solution of NC at pH 7.4 did not show any color change after pH was reduced to 6.8. Note that, as compared with the previous pH-responsive NRs based on channel proteins,[12] this system showed easy preparation and more sensitive response to slight pH change from pH 7.4 to pH 6.8. Further activity measurements confirmed similar maximal reaction velocities (V_{max}) indicating that the encapsulated GOD preserved comparable activity to that of free GOD at pH 6.8 and the self-assembly process for encapsulation did not affect GOD activity obviously (Figure S4). The quantification of released H_2O_2 from *thera*NR demonstrated that H_2O_2 concentration increased to more than 0.3 mM within 1 h at GOD concentration of 100 mU/mL and glucose of 1 mg/mL, which was slightly lower than that of free GOD at pH 6.8 likely due to slightly less efficacious H_2O_2 generation across *thera*NR membranes and consumption by the decomposition of PPBEM segments. However, *thera*NR did not produce any H_2O_2 at pH 7.4 (Figure 1E).

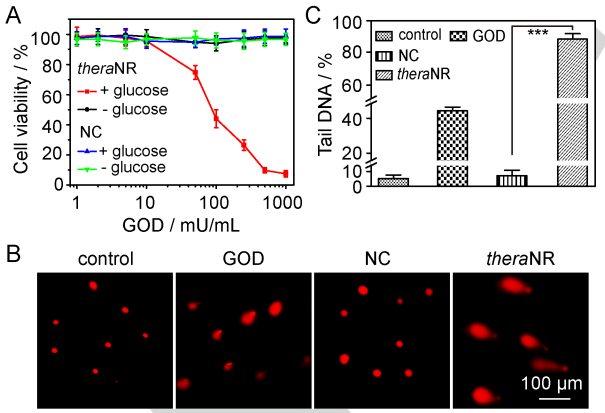

Figure 2. (A) GOD concentration-dependent cytotoxicity of *thera*NRs and NCs without (-) or with (+) glucose (1 mg/mL) at pH 6.8. Mean ± s.d., n = 4. (B) Comet assay and (C) quantitation of tail DNA for control, GOD, NC, and *thera*NR at GOD concentration of 100 mU/mL at pH 6.8. Mean ± s.d., n = 20. ***p < 0.005 (t-test).

On the other hand, with H_2O_2 concentration increasing, high concentration of H_2O_2 will conversely react with PPBEM segments of *thera*NR and degrade the polymers, simultaneously releasing QM as by-products. To evaluate the release profiles of QM, we incubated *thera*NR in the presence of glucose and measured the amount of produced 4-hydroxybenzyl alcohol (HA) as QM can be converted to HA in aqueous solution without other nucleophiles (Figure 1F).[7] At pH 6.8, approximately 60% of QM was released within 72 h, while slight QM was released at pH 7.4. Further morphological observation showed that *thera*NR lost the structural integrity and degraded gradually to pieces of fragments at pH 6.8 after 72 h (Figure S5, SI) whereas no morphological change was observed at pH 7.4 (Figure S6, SI). NC control exhibited no H_2O_2 production and only little QM release at both pH 7.4 and 6.8 (Figure S7, SI). Notably, as shown in Figure 1E, *thera*NR did not show significant H_2O_2 concentration decrease during QM release since only a small quantity of H_2O_2 was consumed. Moreover, in the incubation medium of *thera*NR containing glucose, we added GSH at the concentration of 1 mM. After incubation for 24 h at pH 6.8, the mixture was subjected to liquid chromatography-mass spectrometric (LC-MS) analysis. The product between QM and GSH (QM-GSH) can be detected indicating effective reaction between QM and GSH (Figure S8, SI). Taken together, *thera*NR shows ultra pH-sensitive activation of permeability with pH values changing from 7.4 to 6.8. The nutrients of glucose and oxygen can be converted into H_2O_2 efficiently and release QM from the destruction of the vesicles for GSH depletion (Figure S9, SI).

Cancer cells usually possess deficient reactive oxygen species (ROS)-eliminating systems, which are more sensitive to the elevated oxidative stress than normal cells.[13] On the other hand, cancer cells develop improved antioxidant systems in the tumoral oxidative medium, for example, high concentration of GSH in cytoplasm, thereby rendering them adaptive to the intrinsic oxidative stress in tumor tissue. To evaluate the synergistic effect of *thera*NR on cell viability against cancer cells through massive H_2O_2 production and QM release, we first investigated the intracellular ROS and GSH concentration at pH 6.8 in the medium containing 1 mg/mL glucose. As compared with free GOD and NC, *thera*NR showed significant cellular ROS elevation (Figure S10 SI), and intracellular GSH levels were reduced to 50% and 20% after 24 h and 48 h incubation, respectively (Figure S11, SI). *Thera*NR displayed potent cell killing ability at pH 6.8 (Figure 2A and Figure S12, SI) and induced a high cell death ratio with half maximal inhibitory concentration (IC50) of 87 mU/mL of GOD in *thera*NR at glucose concentration of 1 mg/mL compared with 503 mU/mL of free GOD (Figure S13, SI). Reasonably, compared with free GOD, *thera*NR showed similar H_2O_2 generation ability at pH 6.8, but simultaneously released QM which suppresses the antioxidant capability of cancer cells.[7b] Notably, PEG$_{113}$-*b*-PPBEM$_{80}$ and PEG$_{113}$-*b*-P(PBEM$_{67}$-*co*-PEM$_{23}$) polymers without GOD showed negligible cytotoxicity at the concentration of 1 mg/mL (Figure S14, SI). Moreover, *thera*NR at pH 7.4 and NC at both pH 7.4 and 6.8 all displayed low cytotoxicity due to no membrane permeability (Figure S15, SI). Comet assay was further used to detect DNA damage at the level of the individual cell *via* a pattern of DNA migration by the

electrophoresis gels. Figure 2B,C revealed that *thera*NR severely destroyed the cellular DNA as detected by high ratio of tail DNA ~ 90% compared with ~ 40% of free GOD due to the synergistic effect of *thera*NR on DNA damage of cancer cells.

To evaluate the *in vivo* performance of *thera*NR, A549 tumor-bearing mice were established. *Thera*NR could maintain high stability in the serum-containing medium (Figure S16, SI). Blood circulation test using cypate-labelled GOD (cypate-GOD) revealed long circulation time of *thera*NR with half life of ~ 10 h upon intravenous injection, which is similar to that of NC, whereas free GOD was cleared from the body rapidly (Figure 3A). *In vivo* imaging system (IVIS) was used to investigate the biodistribution of *thera*NR, which showed that *thera*NR had significant tumor accumulation after 12 h post-administration (Figure S17, SI). *Ex vivo* fluorescence images

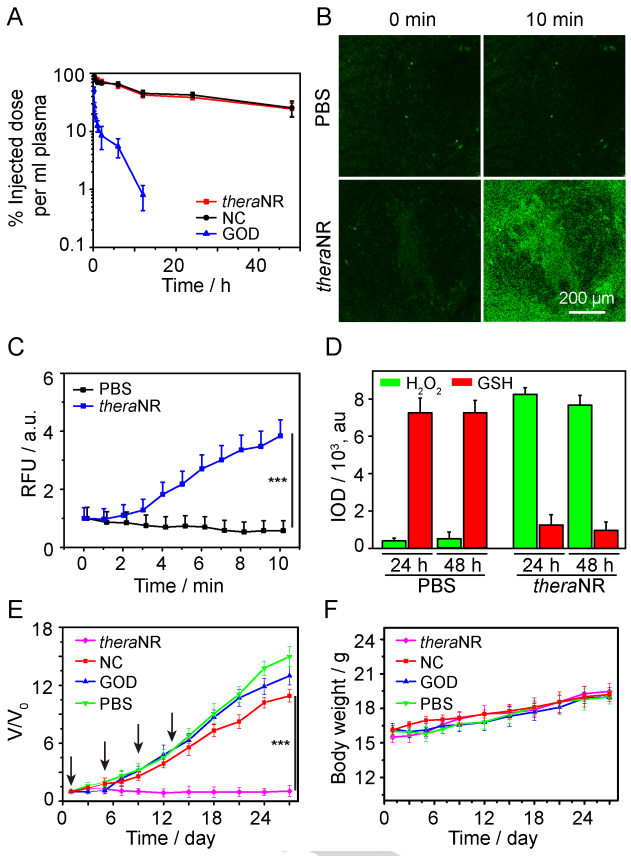

Figure 3. (A) Plasma clearance profiles after *i.v.* injection of cypate-GOD, cypate-GOD-loaded NC, and cypate-GOD-loaded *thera*NR. Mean ± s.d., n = 3. (B) Observation of H_2O_2 distribution in A549 tumor tissues by IVRTCLSM. PBS or *thera*NR was injected into the tail vein of A549 tumor-bearing mice. At 24 h post injection, BES-H_2O_2 was injected into the tail vein of the tumor-bearing mice. (C) Time-dependent relative fluorescence intensity (RFU) in the tumors treated with PBS or *thera*NR. Mean ± s.d., n = 3. ***p < 0.005 (t-test). (D) Quantitation of H_2O_2 and GSH levels in tumor tissue *via* analysis of integrated optical density (IOD) after treatment by PBS or *thera*NR using BES-H_2O_2 and ThiolTracker™ Violet probe, respectively. (E) A549 tumor growth profiles of the mice treated with PBS, GOD, NC, and *thera*NR at GOD dose of 10 U per mouse. Mean ± s.d., n = 5. ***p < 0.005 (t-test). (F) Body weight change of the mice treated with PBS, GOD, NC, and *thera*NR.

after collecting the main organs of the mice at 48 h post injection of NC and *thera*NR loading cypate-GOD displayed significantly stronger fluorescence intensity at tumor sites than other organs indicating high tumor-targeting efficiency of the nanoreactors (Figure S18, SI).

In tumor tissues, the average glucose level is several μM/g tumor tissue and displays heterogeneity,[14] which is the level to guarantee the reaction under the catalysis of the nanoreactors. We first used an intravital confocal microscope (IVRTCLSM) to investigate the generation of H_2O_2 in tumor tissues (Figure S19A, SI). After 24 h post intravenous injection of *thera*NR, 6'-o-pentafluorobenzene sulfonyl-2',7'-difluorofluorescein (BES-H_2O_2) solution was injected into the tail vein and the green fluorescence intensity in tumor was detected using dorsal window chamber models due to the fluorescence turnon after treatment by H_2O_2.[15] The fluorescence intensity increased a factor of four quickly in tumor tissue compared with the PBS, GOD, and NC groups indicating significantly improved H_2O_2 level in tumor after treatment by *thera*NR (Figure 3B,C and Figure S19B,C, SI). Next, we observed H_2O_2 and GSH levels directly in the histological cross sections of the tumor tissue after 24 h and 48 h post intravenous injection of *thera*NR. Upon intratumor injection of BES-H_2O_2 and ThiolTracker™ Violet probe, the corresponding fluorescence intensities revealed that tumor H_2O_2 level was improved to approximately twenty times and GSH concentration was decreased to about one sixth compared with the PBS control (Figure 3D and Figure S20, SI). Notably, we could observe high concentration of H_2O_2 even after 48 h in tumor tissue suggesting that *thera*NR still keep active. Meanwhile, we also used IVRTCLSM to investigate H_2O_2 level in liver and blood circulation upon treatment by *thera*NR. Moreover, after intravenous injection of BES-H_2O_2, we did not observe any H_2O_2 level increase in both liver and blood (Figure S21 and S22, SI). Therefore, we can infer that *thera*NR are inactive in normal tissues at pH 7.4 and work specifically in tumor tissue at pH 6.8.

The synergistic effect of *thera*NR for elevation of oxidative stress and GSH depletion in tumor tissues was expected to finally suppress the tumor growth efficiently. Next, the antitumor efficacy of *thera*NR was investigated using NC, free GOD, and PBS as control groups. As shown in the tumor growth profiles, *thera*NR efficiently inhibit the growth of A549 tumors and even ablate the tumors completely after 27 days treatment (Figure 3E). In sharp contrast, in PBS group, the tumor volume increased to over 12-fold than the original one. In free GOD and NC groups, the tumor sizes were also increased to more than 10 times. The body weights of the mice maintain continual increase during treatment indicated that low systemic toxicity of the therapeutic systems (Figure 3F). Hematoxylin-eosin (H&E) and terminal deoxynucleotidyl transferase dUTP nick end labeling (TUNEL) staining showed large areas of cell apoptosis and tissue necrosis in the tumor tissues treated by *thera*NR group (Figure S23, SI). These results indicated potent antitumor capability of *thera*NR.

In summary, as a proof-of-concept, we constructed *thera*NR with tumor-specific activation and self-destruction based on optimized block copolymer, PEG-*b*-P(PBEM-*co*-PEM), for efficient *in vivo* antitumor application. Proper composition of PPBEM and PPEM endows the formed vesicles with ultra-sensitive pH-responsive permeability while maintaining structural integrity, which makes the vesicles specifically activated at tumor site. The reaction by the

catalysis of *thera*NR occurred in tumor not only consuming the nutrients (glucose and O_2) for H_2O_2 generation, but also releasing QM for GSH depletion. Thus, *thera*NR showed synergistic effect to increase tumor oxidative stress and suppress antioxidative capability of cancer cells, which achieved complete ablation toward A549 tumors while causing negligible systemic toxicity. More details for the antitumor mechanisms of the nanoreactors still need to be studied in future. The design strategy of *thera*NR represents a feasible approach to promote *in vivo* therapeutic application of NRs for maximizing the therapeutic efficacy and minimizing the adverse side effect.

Acknowledgements

We gratefully acknowledge financial support from National Natural Scientific Foundation of China (NNSFC) Project (21674104) and the Fundamental Research Funds for the Central Universities (WK3450000002).

Keywords: nanoreactors • polymersomes • cancer therapy • enzyme delivery • membrane permeability

[1] a) D. M. Vriezema, M. C. Aragones, J. A. A. W. Elemans, J. J. L. M. Cornelissen, A. E. Rowan, R. J. M. Nolte, *Chem. Rev.* **2005**, *105*, 1445-1489; b) J. Gaitzsch, X. Huang, B. Voit, *Chem. Rev.* **2016**, *116*, 1053-1093.

[2] a) A. Ranquin, W. Versees, W. Meier, J. Steyaert, P. Van Gelder, *Nano Lett.* **2005**, *5*, 2220-2224; b) Y. Liu, J. J. Du, M. Yan, M. Y. Lau, J. Hu, H. Han, O. O. Yang, S. Liang, W. Wei, H. Wang, J. M. Li, X. Y. Zhu, L. Q. Shi, W. Chen, C. Ji, Y. F. Lu, *Nat. Nanotechnol.* **2013**, *8*, 187-192; c) P. R. Leduc, M. S. Wong, P. M. Ferreira, R. E. Groff, K. Haslinger, M. P. Koonce, W. Y. Lee, J. C. Love, J. A. McCammon, N. A. Monteiro-Riviere, V. M. Rotello, G. W. Rubloff, R. Westervelt, M. Yoda, *Nat. Nanotechnol.* **2007**, *2*, 3-7.

[3] a) F. Axthelm, O. Casse, W. H. Koppenol, T. Nauser, W. Meier, C. G. Palivan, *J. Phys. Chem. B* **2008**, *112*, 8211-8217; b) Y. Anraku, A. Kishimura, M. Kamiya, S. Tanaka, T. Nomoto, K. Toh, Y. Matsumoto, S. Fukushima, D. Sueyoshi, M. R. Kano, Y. Urano, N. Nishiyama, K. Kataoka, *Angew. Chem. Int. Ed.* **2016**, *55*, 560-565; c) M. Yan, J. J. Du, Z. Gu, M. Liang, Y. F. Hu, W. J. Zhang, S. Priceman, L. L. Wu, Z. H. Zhou, Z. Liu, T. Segura, Y. Tang, Y. F. Lu, *Nat. Nanotechnol.* **2010**, *5*, 48-53.

[4] a) L. Schoonen, J. C. M. van Hest, *Adv. Mater.* **2016**, *28*, 1109-1128; b) P. Tanner, P. Baumann, R. Enea, O. Onaca, C. Palivan, W. Meier, *Acc. Chem. Res.* **2011**, *44*, 1039-1049; c) C. G. Palivan, R. Goers, A. Najer, X. Y. Zhang, A. Car, W. Meier, *Chem. Soc. Rev.* **2016**, *45*, 377-411; d) V. Balasubramanian, B. Herranz-Blanco, P. V. Almeida, J. Hirvonen, H. A. Santos, *Prog. Polym. Sci.* **2016**, *60*, 51-85.

[5] a) M. H. Li, P. Keller, *Soft Matter* **2009**, *5*, 927-937; b) F. H. Meng, Z. Y. Zhong, J. Feijen, *Biomacromolecules* **2009**, *10*, 197-209; c) O. Onaca, R. Enea, D. W. Hughes, W. Meier, *Macromol. Biosci.* **2009**, *9*, 129-139; d) T. Thambi, J. H. Park, D. S. Lee, *Biomater. Sci.* **2016**, *4*, 55-69; e) X. L. Hu, Y. G. Zhang, Z. G. Xie, X. B. Jing, A. Bellotti, Z. Gu, *Biomacromolecules* **2017**, *18*, 649-673; f) Y. Lu, A. A. Aimetti, R. Langer, Z. Gu, *Nat. Rev. Mater.* **2017**, *2*, 16075; g) X. L. Hu, J. C. Yu, C. G. Qian, Y. Lu, A. R. Kahkoska, Z. G. Xie, X. B. Jing, J. B. Buse, Z. Gu, *Acs Nano* **2017**, *11*, 613-620.

[6] a) K. T. Kim, J. J. L. M. Cornelissen, R. J. M. Nolte, J. C. M. van Hest, *Adv. Mater.* **2009**, *21*, 2787-2791; b) J. Gaitzsch, D. Appelhans, L. G. Wang, G. Battaglia, B. Voit, *Angew. Chem. Int. Ed.* **2012**, *51*, 4448-4451; c) Z. Y. Deng, Y. F. Qian, Y. Q. Yu, G. H. Liu, J. M. Hu, G. Y. Zhang, S. Y. Liu, *J. Am. Chem. Soc.* **2016**, *138*, 10452-10466; d) X. R. Wang, G. H. Liu, J. M. Hu, G. Y. Zhang, S. Y. Liu, *Angew. Chem. Int. Ed.* **2014**, *53*, 3138-3142; e) M. Spulber, A. Najer, K. Winkelbach, O. Glaied, M. Waser, U. Pieles, W. Meier, N. Bruns, *J. Am. Chem. Soc.* **2013**, *135*, 9204-9212; f) Q. Yan, J. B. Wang, Y. W. Yin, J. Y. Yuan, *Angew. Chem. Int. Ed.* **2013**, *52*, 5070-5073; g) C. G. Qian, P. J. Feng, J. C. Yu, Y. L. Chen, Q. Y. Hu, W. J. Sun, X. Z. Xiao, X. L. Hu, A. Bellotti, Q. D. Shen, Z. Gu, *Angew. Chem. Int. Ed.* **2017**, *56*, 2588-2593; h) K. Renggli, P. Baumann, K. Langowska, O. Onaca, N. Bruns, W. Meier, *Adv. Funct. Mater.* **2011**, *21*, 1241-1259.

[7] a) K. E. Broaders, S. Grandhe, J. M. J. Frechet, *J. Am. Chem. Soc.* **2011**, *133*, 756-758; b) J. Noh, B. Kwon, E. Han, M. Park, W. Yang, W. Cho, W. Yoo, G. Khang, D. Lee, *Nat. Commun.* **2015**, *6*, 6907.

[8] a) N. Hulsman, J. P. Medema, C. Bos, A. Jongejan, R. Leurs, M. J. Smit, I. J. P. de Esch, D. Richel, M. Wijtmans, *J. Med. Chem.* **2007**, *50*, 2424-2431; b) H. Hagen, P. Marzenell, E. Jentzsch, F. Wenz, M. R. Veldwijk, A. Mokhir, *J. Med. Chem.* **2012**, *55*, 924-934.

[9] T. Chang, M. S. Lord, B. Bergmann, A. Macmillan, M. H. Stenzel, *J. Mater. Chem. B* **2014**, *2*, 2883-2891.

[10] a) K. J. Zhou, H. M. Liu, S. R. Zhang, X. N. Huang, Y. G. Wang, G. Huang, B. D. Sumer, J. M. Gao, *J. Am. Chem. Soc.* **2012**, *134*, 7803-7811; b) K. J. Zhou, Y. G. Wang, X. N. Huang, K. Luby-Phelps, B. D. Sumer, J. M. Gao, *Angew. Chem. Int. Ed.* **2011**, *50*, 6109-6114.

[11] P. D. Josephy, T. Eling, R. P. Mason, *J. Biol. Chem.* **1982**, *257*, 3669-3675.

[12] T. Einfalt, R. Goers, I. A. Dinu, A. Najer, M. Spulber, O. Onaca-Fischer, C. G. Palivan, *Nano Lett.* **2015**, *15*, 7596-7603.

[13] a) D. Trachootham, J. Alexandre, P. Huang, *Nat. Rev. Drug Discovery* **2009**, *8*, 579-591; b) J. Fang, T. Seki, H. Maeda, *Adv. Drug Delivery Rev.* **2009**, *61*, 290-302.

[14] a) P. Vaupel, *Semin. Radiat. Oncol.* **2004**, *14*, 198-206; b) T. Schroeder, H. Yuan, B. L. Viglianti, C. Peltz, S. Asopa, Z. Vujaskovic, M. W. Dewhirst, *Cancer Res.* **2005**, *65*, 5163-5171.

[15] a) J. J. Li, W. D. Ke, L. Wang, M. M. Huang, W. Yin, P. Zhang, Q. X. Chen, Z. S. Ge, *J. Controlled Release* **2016**, *225*, 64-74; b) H. Maeda, Y. Futkuyasu, S. Yoshida, M. Fukuda, K. Saeki, H. Matsuno, Y. Yamauchi, K. Yoshida, K. Hirata, K. Miyamoto, *Angew. Chem. Int. Ed.* **2004**, *43*, 2389-2391.

10.1002/anie.201706964

WILEY-VCH

Entry for the Table of Contents

Layout 1:

COMMUNICATION

***In vivo* therapeutic nanoreactors (*thera*NR)**: Glucose oxidase (GOD)-loaded vesicular *thera*NR are engineered to be specifically activated by tumor acidity and produce H_2O_2 for improving the tumor oxidative stress. High level of H_2O_2 induces vesicle self-destruction and release of quinone methide to deplete glutathione and suppress antioxidant ability of cancer cells. The synergistic effect of *thera*NR results in efficient cancer cell killing and tumor ablation.

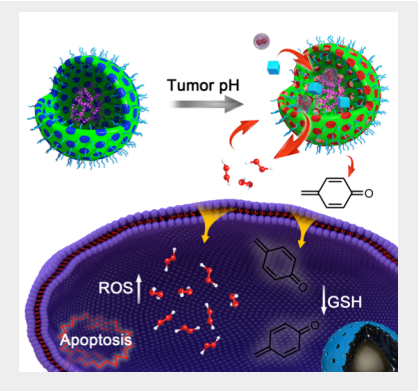

Junjie Li, Anjaneyulu Dirisala, Zhishen Ge, Yuheng Wang, Wei Yin, Wendong Ke, Kazuko Toh, Jinbing Xie, Yu Matsumoto, Yasutaka Anraku,* Kensuke Osada,* and Kazunori Kataoka**

Page No. – Page No.

Therapeutic Vesicular Nanoreactors with Tumor-Specific Activation and Self-Destruction for Synergistic Tumor Ablation